Supplementary Materials for

Structure of a class C GPCR metabotropic glutamate receptor 1 bound to an allosteric modulator

Huixian Wu,[1*] Chong Wang,[1*] Karen J. Gregory,[2,3] Gye Won Han,[1] Hyekyung P. Cho,[2] Yan Xia,[4] Colleen M. Niswender,[2] Vsevolod Katritch,[1] Jens Meiler,[4] Vadim Cherezov,[1] P. Jeffrey Conn,[2] Raymond C. Stevens[1⊥]

correspondence to: stevens@scripps.edu

This PDF file includes:

Materials and Methods

Generation of BRIL-mGlu$_1$TM fusion constructs for *Spodoptera frugiperda* (*Sf*9) expression

A thermally stabilized apocytochrome b_{562}RIL (*38*) was fused to the N-terminus of the human mGlu$_1$ receptor 7TM domain at I581 using overlapping PCR. The C-terminus was truncated at V860 (as shown in Fig. S1). The receptor chimera sequence was subcloned into a modified pFastBac1 vector (Invitrogen), designated as pFastBac1-833100, which contained an expression cassette with a haemagglutinin (HA) signal sequence followed by a Flag tag, a 10× His tag, and a TEV protease recognition site at the N-terminus before the receptor sequence. Subcloning into the pFastBac1-833100 was achieved using PCR with primer pairs encoding restriction sites KpnI at the 5′ and HindIII at the 3′ termini with subsequent ligation into the corresponding restriction sites found in the vector.

Expression and purification of mGlu$_1$ protein for crystallization

High-titer recombinant baculovirus (>10^9 viral particles per ml) was obtained using the Bac-to-Bac Baculovirus Expression System (Invitrogen) as previously described (*16*). Cell suspensions were incubated for 4 days while shaking at 27 °C. *Sf*9 cells at a cell density of 2–3 × 10^6 cells ml^{-1} were infected with P2 virus at a m.o.i. (multiplicity of infection) of 5. Cells were harvested by centrifugation at 48 h post-infection and stored at −80 °C until use.

Insect cell membranes were disrupted by thawing frozen cell pellets in a hypotonic buffer containing 10 mM HEPES (pH 7.5), 10 mM $MgCl_2$, 20 mM KCl and EDTA-free complete protease inhibitor cocktail tablets (Roche). Extensive washing of the raw membranes was performed by repeated centrifugation in the same hypotonic buffer (2-3 times), and then in a high osmotic buffer containing 1.0 M NaCl, 10 mM HEPES (pH 7.5), 10 mM $MgCl_2$, 20 mM KCl and EDTA-free complete protease inhibitor cocktail tablets (3-4 times), thereby separating soluble and membrane associated proteins from integral transmembrane proteins.

Washed membranes were resuspended into a buffer containing 15 μM FITM, 2 mg ml^{-1} iodoacetamide, and EDTA-free complete protease inhibitor cocktail tablets, and incubated at 4 °C for 1 h before solubilization. The membranes were then solubilized in 50 mM HEPES (pH 7.5), 200 mM NaCl, 1% (w/v) n-dodecyl-β-D-maltopyranoside (DDM, Anatrace), 0.2% (w/v) cholesteryl hemisuccinate (CHS, Sigma) at 4 °C. The supernatant was isolated by centrifugation at 160,000g for 30 min, and incubated in 20 mM buffered imidazole (pH 7.5), 800 mM NaCl with TALON IMAC resin (Clontech) overnight at 4 °C. After binding, the resin was washed with 10 column volumes of Wash I Buffer (50 mM HEPES (pH 7.5), 800 mM NaCl, 10 μM FITM, 10% (v/v) glycerol, 0.1% (w/v) DDM, 0.02% (w/v) CHS, 10 mM ATP and 10 mM $MgCl_2$), followed by 6 column volumes of Wash II Buffer (50 mM HEPES (pH 7.5), 500 mM NaCl, 10 μM FITM, 10% (v/v) glycerol, 0.05% (w/v) DDM, 0.01% (w/v) CHS). The protein was then eluted by 3-4 column volumes of Elution Buffer (50 mM HEPES (pH 7.5), 10 μM FITM, 500 mM NaCl, 10% (v/v) glycerol, 0.05% (w/v) DDM, 0.01% (w/v) CHS, and 250 mM imidazole). PD MiniTrap G-25 column (GE Healthcare) was used to remove imidazole. The protein was then treated overnight with His-tagged TEV protease to cleave the N-terminal His-tag and Flag-tag. TEV protease and cleaved N-terminal fragment were

removed by binding to TALON IMAC resin for 2 h at 4 °C. The tag-less protein was collected as the TALON IMAC column flow-through. The protein was then concentrated to 50-80 mg/ml with a 100 kDa molecular weight cut-off Vivaspin centrifuge concentrator (GE Healthcare).

Lipidic cubic phase crystallization

Protein samples were reconstituted into lipidic cubic phase (LCP) by mixing with molten lipid constituted by 90% (w/w) of monoolein and 10% (w/w) of cholesterol in a mechanical syringe mixer (39). LCP crystallization trials were performed in 96-well glass sandwich plates (Marienfeld) using an NT8-LCP crystallization robot (Formulatrix) as previously described (*16*). Plates were incubated and imaged at 20 °C using an automated incubator/imager (RockImager 1000, Formulatrix). Initial crystal hits were obtained from a precipitant condition containing 100 mM HEPES (pH 7.0), 30% (v/v) PEG400, 100 mM $(NH_4)_2HPO_4$ in LCP-Fluorescence Recovery After photobleaching (LCP-FRAP) experiment (*40*). Crystals for data collection were grown in 100 mM HEPES (pH 7.0), 27-30% (v/v) PEG400, 80-120 mM $(NH_4)_2HPO_4$ and 4-8 mM TCEP. Crystals reached full size (35 μm × 35 μm × 15 μm) within 5-6 days and were harvested directly from LCP matrix using MiTeGen micromounts and flash frozen in liquid nitrogen.

Crystallographic data collection and processing.

X-ray data were collected at the 23ID-D beamline (GM/CA CAT) at the Advanced Photon Source, Argonne, IL using a 20 μm minibeam at a wavelength of 1.0332 Å and a MarMosaic 300 CCD detector. Crystals were aligned and data were collected using strategy similar to other GPCR structures (*41*). Typically 20 frames at 1° oscillation and 1 s exposure with non-attenuated beam were collected following by a translation of the crystal to a non-exposed position or changing the crystal to minimize the effect of radiation damage. A complete data set was obtained by indexing, integrating, scaling, and merging data from 14 crystals using HKL2000 (42) (Table S1).

Experimental phasing

The attempts to find a molecular replacement solution using an ensemble of all previous class A GPCR structures as a search model did not generate any reliable solutions. Therefore, experimental phasing was performed by soaking the crystals in the presence of 5 mM tantalum bromide cluster (Ta_6Br_{14}, Jena Bioscience) for 24 h. The single wavelength anomalous data (SAD) were collected at 23ID-D beamline (GM/CA CAT) at the Advanced Photon Source using the peak wavelength of the tantalum L3 edge (9.880 keV). A complete 360° data set was acquired from a single crystal by using a 20 μm minibeam at 50 × attenuation with 1° oscillation and 1 s exposure per frame and collecting 30° wedges with direct and inverse beam. The SAD data set was integrated and scaled at 4.0 Å resolution using HKL2000, and PHENIX.AutoSol (*43*) was used to search for the heavy atom sites.

Structure determination and refinement

The structure was initially solved using 4.0 Å Ta SAD data with PHENIX.AutoSol, the map clearly showed TM helices. Further heavy atom refinement and phasing, combining the 2.8 Å resolution native data, a set of 3.5 Å resolution data collected on 8

tantalum bromide soaked crystals at 1.0332 Å wavelength, and the SAD data and SAD (SIRAS) was carried out using SHARP (*44*) based on two heavy atom sites identified from the anomalous difference map. Density modification and automatic tracing were then performed using PHENIX.AutoBuild (*45*). Refinement was performed by rounds of REFMAC5 (*46*) and autoBUSTER (*47*) using the 2.8 Å resolution native dataset followed by manual examination and rebuilding of the refined coordinates in the program COOT (*48*) using both $|2F_o|$ - $|F_c|$ and $|F_o|$ - $|F_c|$ maps, as well as omit maps. Data collection and refinement statistics are shown in Table S1.

T-REx^{TM}-293 cell transfection and cell culture and mutation generation

The human $mGlu_1$ full-length open reading frame ($mGlu_1$-WT) was amplified from a human brain cDNA library (Clontech Laboratories, Mountain View, CA) and cloned into the BamH1 and Xho I sites of a tetracycline-inducible mammalian expression vector, pcDNA5/TO (Life Technologies, Carlsbad, CA). The human mGlu1 transmembrane construct for crystallization ($mGlu_1$-TM) from pFASTbac1 was subcloned into the BamH1 and NotI sites of pcDNA5/TO. To generate stable cell lines expressing $mGlu_1$-WT and $mGlu_1$-TM, T-REx^{TM}-293 cells (Life Technologies, Carlsbad, CA) were transfected with these respective expression plasmids using Fugene 6 (Promega, Madison, WI). Two days after transfection, the cells were incubated in selection medium containing 200 µg/ml hygromycin, and 10 µg/ml Blasticidin S to maintain Tet Repressor expression. The resulting polyclonal T-REx^{TM}-293 cells were cultured in Dulbecco's Modified Eagle Medium (DMEM) growth medium containing 10% Tet-tested fetal bovine serum (Atlanta Biologicals, Flowery Branch, GA). The day before calcium assays and membrane preps for radioligand binding assays, 1 µg/ml tetracycline was added to induce receptor expression. The human $mGlu_5$ expressing cells were cultured as described (*49*). Site-directed mutagenesis of human $mGlu_1$ pcDNA5/TO was performed using a QuikChange II XL kit (Agilent Tech., Santa Clara, CA). All mutants were sequenced to confirm the presence of corresponding point-mutation sites and assessed for pharmacological activity 48 h after transient transfection.

Radioligand binding

Membranes from *Sf*9 cells and T-REx^{TM}-293 cells expressing $mGlu_1$-WT or $mGlu_1$-TM were prepared as described (*50*). Briefly, for saturation binding assays, membranes (10 µg) were incubated with a varying range of [^{3}H]-R214127 (0.16-20 nM, 25 Ci/mmol) in binding buffer (50 mM Tris-HCl, 1.2 mM $MgCl_2$, and 2 mM $CaCl_2$, pH 7.4). Non-specific binding was determined in the presence of 10 µM JNJ16259685 (ref (*51*)). For competition binding assays with $mGlu_1$-WT and $mGlu_1$-TM, membranes (10 µg) were incubated with 3 nM of [^{3}H]-R214127 with a varying concentration of FITM. For $mGlu_5$ experiments, membranes (20 µg) were incubated with 3 nM of [^{3}H]-methoxyPEPy and nonspecific binding was determined using 10 µM MPEP as described (*30*). All $mGlu_1$ binding experiments were performed on ice for 1 h and $mGlu_5$ experiments were performed at room temperature. Binding was terminated by rapid filtration through GF/B Unifilter plates (PerkinElmer Life and Analytical Sciences, Boston, MA) using a Brandel 96-well plate Harvester (Brandel Inc., Gaithersburg, MD), followed by three washes with ice-cold harvesting buffer (25 mM Tris-HCl, pH 7.4, 150 mM NaCl). Plates were air

dried overnight, Microscint20 added and radioactivity counted using a TopCount Scintillation Counter (PerkinElmer Life and Analytical Sciences).

Calcium mobilization

To measure the functional activity of $mGlu_1$-TM, the $mGlu_1$ PAM RO0711401 was used to activate the truncated and full-length receptors using calcium mobilization assays. Briefly, the day before the assay, stable T-REx^{TM}-293 cells were plated in DMEM containing 10% dialyzed fetal bovine serum, 20 mM HEPES, 100 units/mL penicillin/streptomycin, 1 mM sodium pyruvate and 1 μg/ml tetracycline to induce receptor expression. Cells were plated in black-walled, clear-bottomed, poly-D-lysine coated, 384 well plates (Greiner Bio-One, Monroe, NC) and grown overnight at 37 °C in the presence of 5% CO2. During the day of assay, the medium was replaced with 20 μL of 1 μM Fluo-4-acetomethoxyester (Fluo-4-AM) prepared as a 2.3 mM stock in DMSO and mixed in a 1:1 ratio with 10% (w/v) pluronic acid F-127 and diluted to 1.15 μM final in Assay Buffer (Hank's balanced salt solution, 20 mM HEPES, 2.5 mM Probenecid) for 45 min at 37 °C. Dye was removed and replaced with Assay Buffer. Calcium flux was measured using the Functional Drug Screening System 7000 (FDSS7000, Hamamatsu, Japan). Baseline readings were taken (10 images at 1 Hz, excitation, 470 ± 20 nm, emission, 540 ± 30 nm) and then an appropriate concentration of vehicle or FITM was added; cells were incubated for 2 min before application of RO0711401 and calcium responses were measured. The maximal calcium response, minus a local minima calculated immediately before the RO0711140 was added, was calculated and curves were fitted using a four point logistical equation in GraphPad Prism5.0 (GraphPad Software, Inc., La Jolla, CA). All reagents used were from Life Technologies (Carlsbad, CA) unless otherwise noted.

Allosteric modeling

Shifts of agonist concentration-response curves at WT and mutant human $mGlu_1$ receptors by FITM were globally fitted to an operational model of allosterism (*52*):

$$y = basal + \frac{(E_m - basal)(\tau_A[A](K_B + \alpha\beta[B]) + \tau_B[B]K_A)^n}{(\tau_A[A](K_B + \alpha\beta[B]) + \tau_B[B]K_A)^n + ([A]K_B + K_AK_B + K_A[B] + \alpha[A][B])^n}$$

where A is the molar concentration of the orthosteric agonist; B is the molar concentration of the allosteric modulator; KA is the equilibrium dissociation constant of the orthosteric agonist glutamate, and KB is the equilibrium dissociation constant of allosteric modulator. Affinity modulation is governed by the cooperativity factor α, and efficacy modulation is governed by β. The parameters τA and τB relate to the ability of orthosteric agonist and allosteric ligands, respectively, to directly activate the receptor. Basal, Em and n represent the basal system response, maximal possible system response and the transducer function that links occupancy to response.

For the analysis of effect of mutation on FITM, the logK_A of glutamate for $mGlu_1$ was constrained to the observed potency at the WT $mGlu_1$ receptor (-6.337) as the affinity of glutamate for human $mGlu_1$ is unknown. With few exceptions, log τβ and log β were set to -100 and log α was constrained to 0 for all mutants as previously validated for $mGlu_5$ (*30*); this reflects the lack of allosteric agonism (τβ), and complete blockade of glutamate (β). The exceptions to use of these parameters were for point mutants

S668$^{3.36}$P, P756$^{5.43}$S, and T815$^{7.38}$M where log α and log β were not constrained due to evidence of incomplete blockade of the glutamate response.

Compounds

[^{3}H]-R214127 was custom synthesized by American Radiolabeled Chemicals (St. Louis, MO) and [^{3}H]-methoxyPEPy was custom synthesized by PerkinElmer Life and Analytical Sciences. RO0711401 (*53*) and FITM (*54*) were synthesized at Vanderbilt University Medical Center using methods analogous to those found in ref (*55*), RO0711401=compound "14a" in ref (*55*); FITM=compound "27" in ref (*9*). Compound structures were confirmed by ^{1}H-NMR and analytical LCMS.

Computational ligand docking in FITM binding pocket

FITM and five derivatives reported by Satoh et al (*9*) were computationally docked into the $mGlu_1$ using RosettaLigand (*37, 56*). The Ligand conformers were generated using MOE (*57*) (Molecular Operating Environment; Chemical Computing Group Inc., Montreal, QC, Canada). The ligands are placed into the binding pocket, superimposing the large common substructure with the experimentally determined FITM coordinates. 1000 docking models per compound were constructed with 2Å translational and 10° rotational sampling (*31, 37*). We limited sampling to retain the experimentally determined FITM binding mode for all derivatives. Resulting models were ranked based on their predicted binding energy using an energy function that contains terms for van der Waals attractive and repulsive forces, electrostatic interactions, hydrogen bonding, solvation, and likelihood of particular side-chain conformations. The ligand interface energy of the top 1% scoring models was used to compute the predicted ensemble average ligand binding energy and to correlate with experimental IC_{50}. The predicted per residue binding energy was extracted from top 1% models where negative values indicate residues that contribute favorable interactions, positive values indicate residues that contribute unfavorable interactions, zero values indicate residues not involved in ligand binding. The top scoring docked model is used for visualizing ligand-protein interface in PyMol.

Full-length model building

The ECD of $mGlu_1$ was constructed by homology modeling of the glutamate-bound dimeric VFD structure from $mGlu_1$ (PDB ID: 1EWK) and CRD from $mGlu_3$ (PDB ID: 2E4U) using Rosetta (M1, M2). The model was constructed imposing a perfect 2-fold rotational symmetry (M3). For this purpose, the template 1EWK which is in a putative Aco (active closed-open) conformation was converted into a symmetric Acc (active closed-closed) conformation before the CRDs were added. To bring the CRDs into intimate contact (*34*) the loop region between Q513 and V523 and the C254-C543 disulfide bond were remodeled to allow the relative orientation of CRD and VFD to be sampled. The ECD was placed with its C-termini P580 within 4Å distance to I581, the N-terminal residue of the 7TM domain, imposing C2 symmetry. The loop region E579 to P582 was reconstructed to link the CRD and 7TM domain.

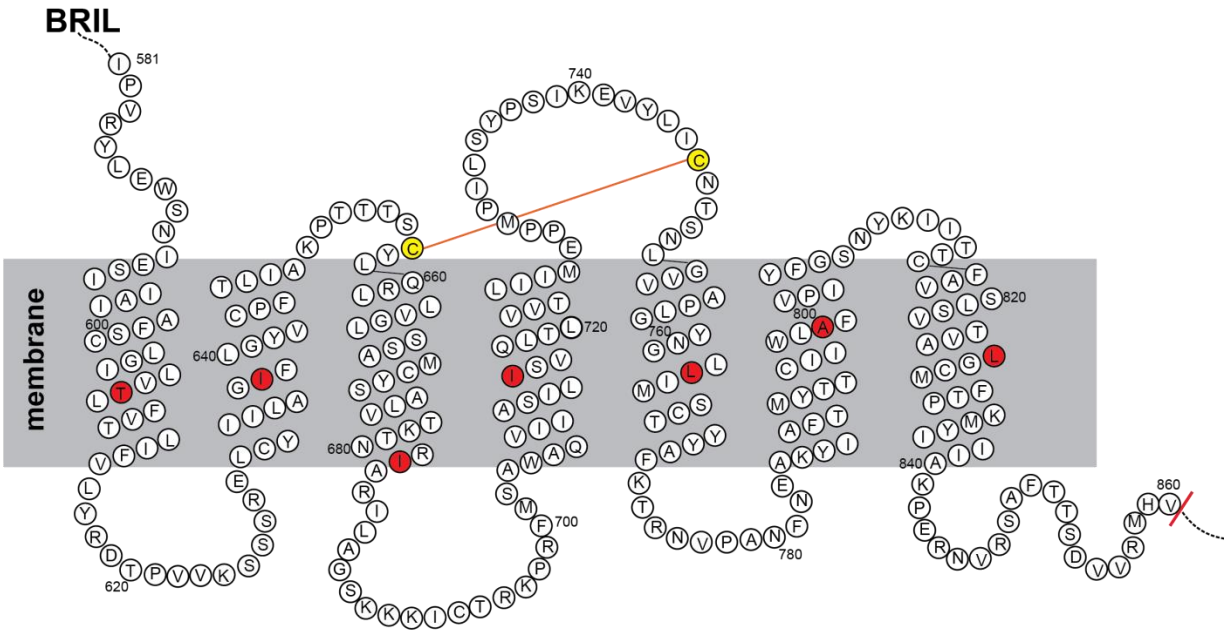

Fig. S1.

Snake plot representation of the $mGlu_1$ 7TM domain. Residues that are superposed to X.50 (B&W numbering) of class A GPCRs (see Fig. S7 for the superposition) are labeled as red circles.

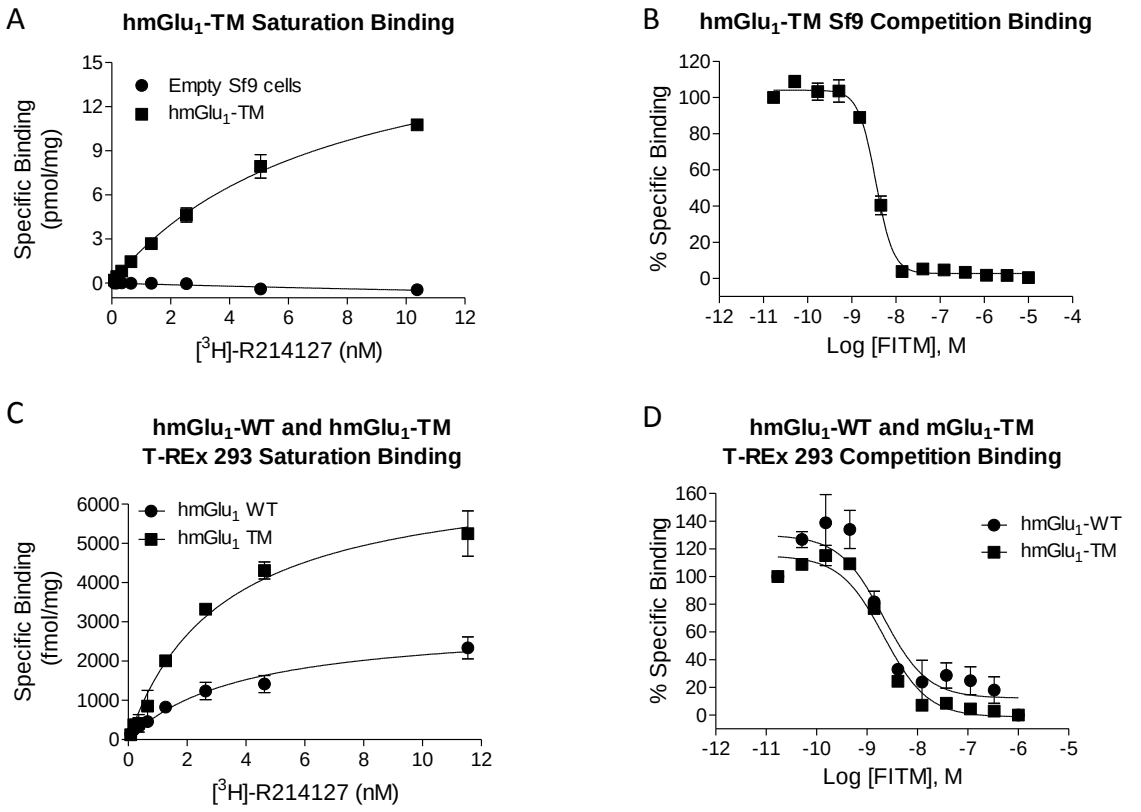

Fig. S2

The human $mGlu_1$ ($hmGlu_1$) TM construct binds an $mGlu_1$-selective radioligand in a saturable fashion when expressed in *Sf*9 and HEK cells and the $mGlu_1$ negative allosteric modulator FITM fully displaces radioligand binding. (A) Membranes were prepared from Sf9 cells expressing $hmGlu_1$-TM and saturation binding was performed using increasing concentrations of the $mGlu_1$ radioligand [^{3}H]-R214127 (squares, ref (58)). Membranes from untransfected *Sf*9 cells were used as a control (circles). The $hmGlu_1$-TM was capable of binding [^{3}H]-R214127 in a saturable fashion; the Bmax was calculated to be 17.5 ± 1.6 pmol/mg and the Kd for [^{3}H]-R214127 was 3.8 ± 1.9 nM. Data shown are from one experiment that is representative of three independent experiments performed in triplicate. (B) Competition binding was performed using *Sf*9 cells expressing $hmGlu_1$-TM. Increasing concentrations of FITM were incubated with 3 nM [^{3}H]-R214127 for 1hr on ice. FITM fully displaced [^{3}H]-R214127 with a K_i of 2.5 ± 0.23 nM. Data represent the mean ± SEM of three independent experiments performed in triplicate. (C) To determine if $hmGlu_1$-TM could interact with both [^{3}H]-R214127 and FITM in mammalian cells, full-length human $mGlu_1$ ($hmGlu_1$-WT) and the $hmGlu_1$-TM construct were cloned into the tetracycline-inducible vector pcDNA5/TO, and used for generating tetracycline-inducible stable cells in T-REx^{TM}-293 cells. Membranes were prepared from T-REx^{TM}-293 cells stably expressing either $hmGlu_1$-WT or $hmGlu_1$-TM that had been induced with 1 µg/mL of tetracycline; saturable [^{3}H]-R214127 binding was identified for both proteins with similar affinity ($hmGlu_1$-WT, B_{max}, 2734 ± 135 fmol/mg, K_d, 3.0 ± 0.4 nM and $hmGlu_1$-TM, B_{max}, 6811 ± 832 fmol/mg, K_d, 3.2 ± 0.5 nM; K_d values between $hmGlu_1$-WT and $hmGlu_1$-TM, p=0.795, unpaired t-test). Data shown are from one

experiment that is representative of three independent experiments performed in triplicate. (D) Competition binding was performed using T-REx^{TM}-293 cell membranes expressing either hmGlu$_1$-WT or hmGlu$_1$-TM. Increasing concentrations of FITM were incubated with 3 nM [^{3}H]-R214127 and filter binding was performed. FITM fully displaced the binding of [^{3}H]-R214127 from membranes expressing hmGlu$_1$-WT and hmGlu$_1$-TM with comparable affinities (K_i for FITM was 1.36 ± 0.13 nM for hmGlu$_1$-WT and 1.41 ± 0.02 nM for hmGlu$_1$-TM, p=0.726, unpaired t-test). Data represent the mean ± SEM of three independent experiments performed in at least triplicate.

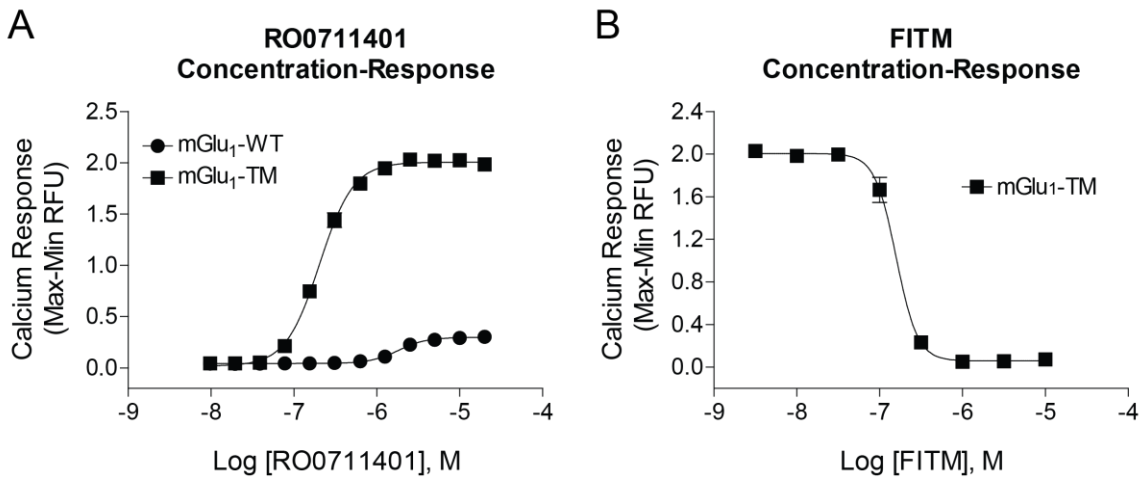

Fig. S3

The $mGlu_1$-TM functionally responds to both positive and negative allosteric modulators of $mGlu_1$. After determining the binding affinity of FITM, we next performed calcium mobilization assays with cells expressing each receptor variant to ensure that the truncated receptor was functional. Due to the lack of the VFD, the truncated construct does not respond to glutamate or other orthosteric agonists; however, it has been shown that positive allosteric modulators (PAMs) can directly activate truncated versions of mGlus (*59*). Therefore, we used the $mGlu_1$ PAM RO0711401 as an agonist for these studies. (A) $mGlu_1$-WT (circles) and $mGlu_1$-TM (squares) were expressed in T-REx^{TM}-293 cells and induced overnight with 1 µg/mL of tetracycline. Increasing concentrations of the $mGlu_1$ PAM RO0711401 were applied and calcium responses were measured. Potencies of RO0711401 at $mGlu_1$-WT and $mGlu_1$-TM were 1.7 ± 0.2 µM and 190 ± 27 nM, respectively ($p=0.001$, Student's t-test); the reduced potency and efficacy at the WT receptor is consistent with the dominant ability of the VFD to dampen the inherent allosteric agonist activity induced by PAMs. (B) Increasing concentrations of FITM were applied 2 min prior to the application of 10 µM RO0711401 and blockade of calcium responses downstream of $mGlu_1$-TM was measured; FITM IC_{50} in this assay was 161 ± 14 nM. Data for both panels represent the mean ± SEM of three independent experiments performed in at least triplicate.

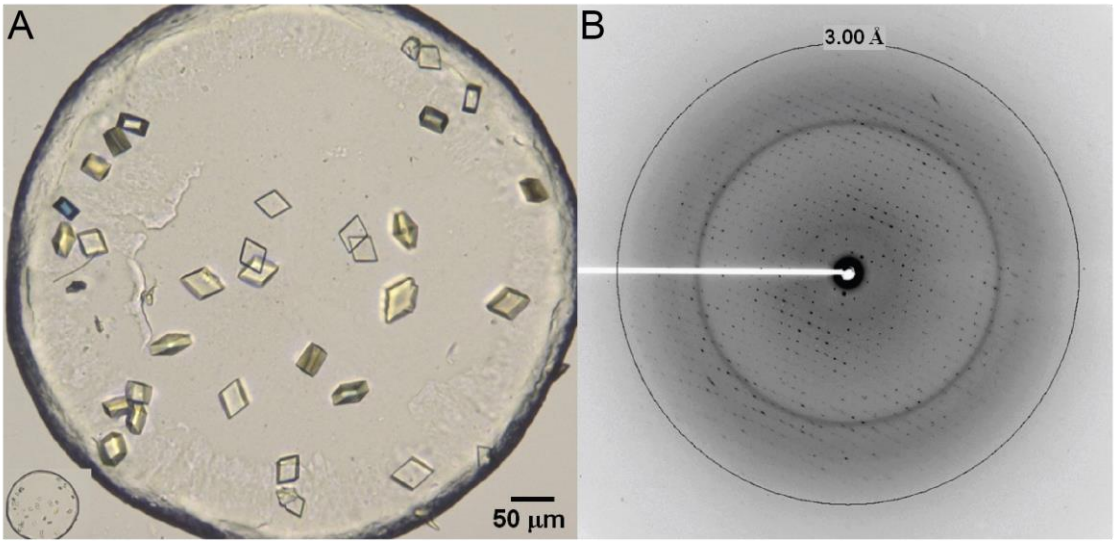

Fig. S4
Images of BRIL-mGlu$_1$/NAM crystals (A) and representative diffraction pattern (B).

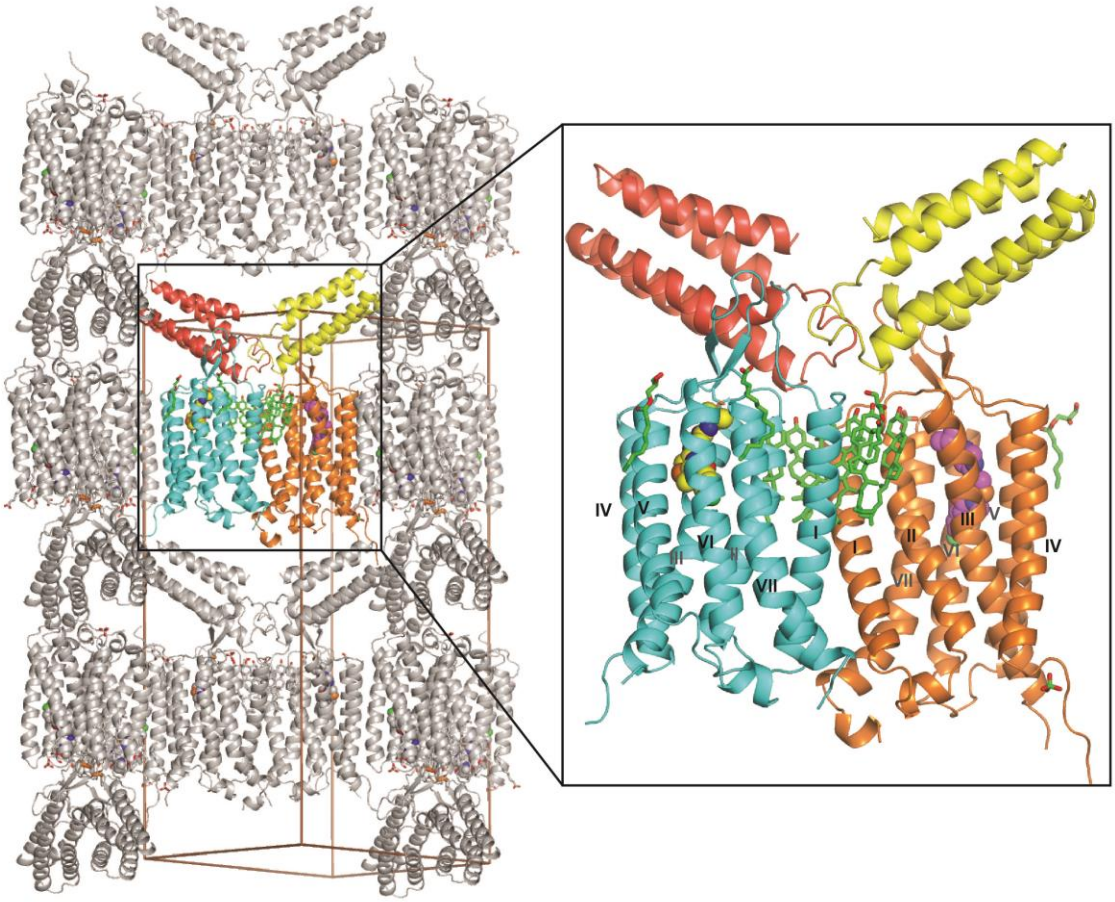

Fig. S5

Crystal packing of the BRIL-mGlu$_1$/NAM complex. Shown in the center of the crystal packing diagram and in the enlarged insert on the right is one asymmetric unit which contains a parallel dimer. In molecule A, receptor is colored cyan with ligand shown as yellow carbons, and BRIL is colored red; in molecule B, receptor is colored orange with ligand shown as magenta carbons, and BRIL is colored yellow. Cholesterols and lipids are shown as green carbons. The images were created with PyMOL.

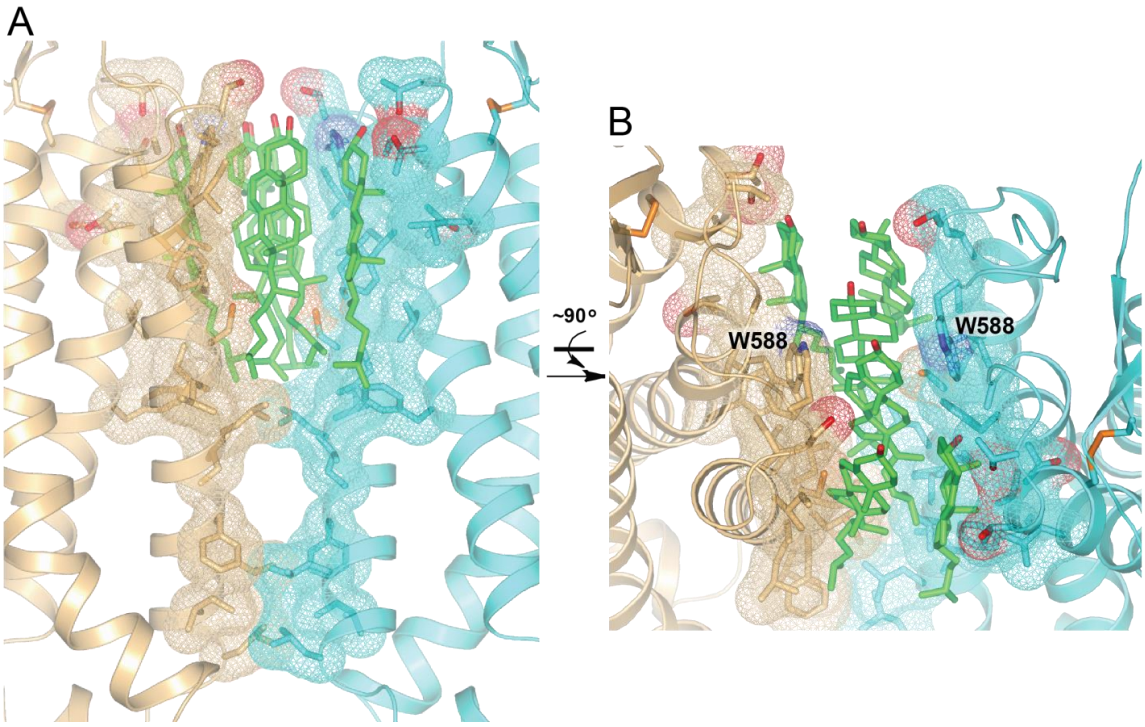

Fig. S6

$mGlu_1$ dimer interface observed in the crystal structure. Molecule A is colored cyan; molecule B is colored light orange. Cholesterols which mediate the dimer formation are shown as green carbons. Residues participating in receptor-cholesterol interactions and receptor-receptor interactions are shown in sticks and surface presentation. W588 which is conserved in all mGlus and packs to cholesterol molecules is labeled. The images were created with PyMOL.

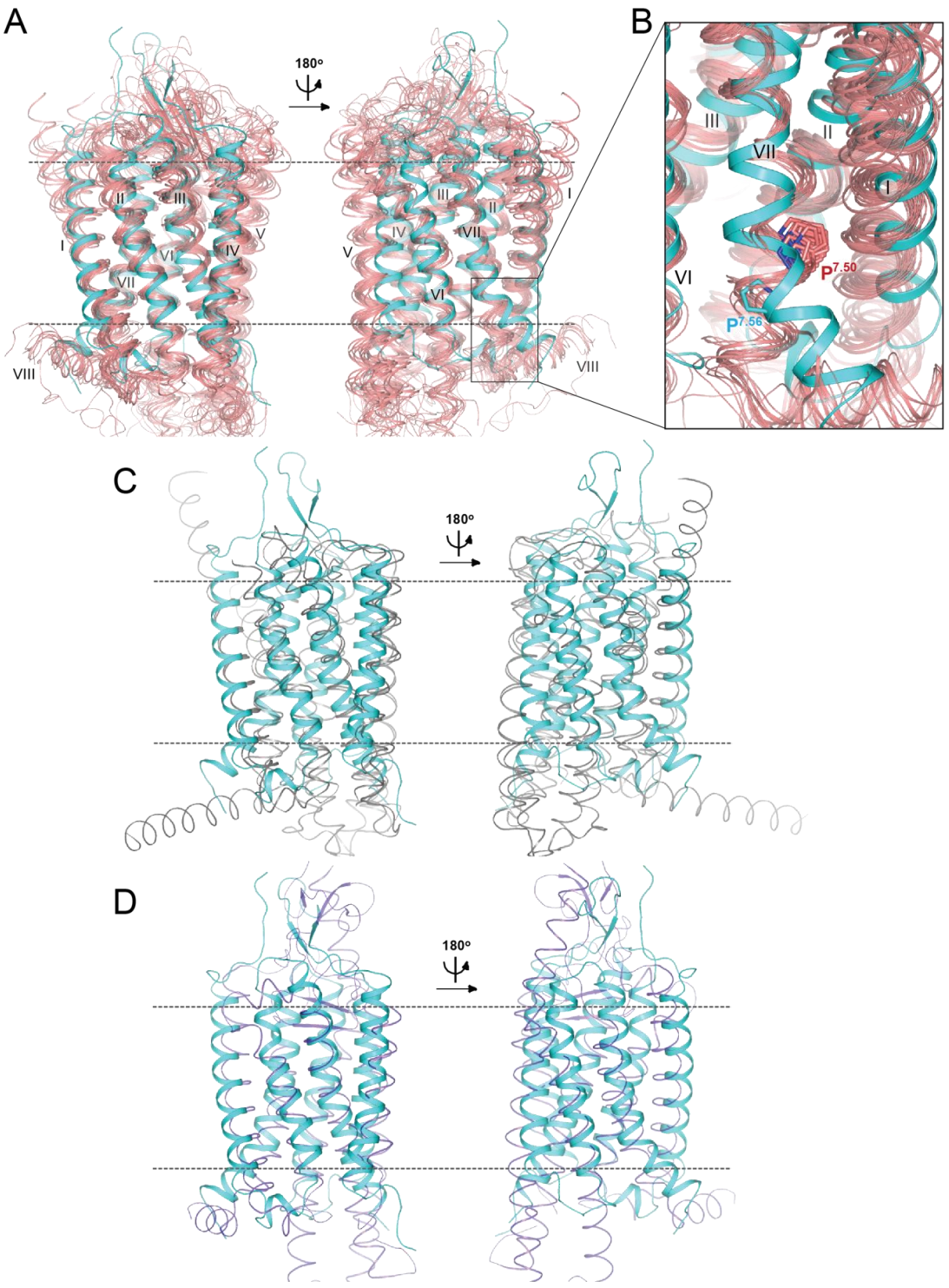

Fig. S7

7TM domain comparison of $mGlu_1$ with classes A, B and F GPCRs. (A) Side views of the superposition of $mGlu_1$ (cyan) with class A GPCRs (salmon). (B) Superposition of the intracellular end of helix VII of $mGlu_1$ with class A GPCRs. $P^{7.50}$ of class A GPCRs is shown in sticks with carbons colored in salmon. $P833^{7.56}$ of $mGlu_1$ is shown in sticks with

cyan carbons. (C) Side views of the superimposition of $mGlu_1$ with class B GPCRs (CRFR1 and glucagon receptor; PDB ID 4K5Y and 4L6R, respectively) shown in black. (D) Side views of the superposition of $mGlu_1$ with class F GPCR, smoothened receptor (PDB ID 4JKV) shown in purple. Structures of class A GPCRs used in (A) and (B) include PDB IDs: 1U19, 2RH1, 2YCW, 3RZE, 3PBL, 3UON, 4DAJ, 3EML, 3V2W, 3ODU, 4DJH, 4EA3, 4DKL, 4EJ4, 3VW7, 4GRV. The images were created with PyMOL.

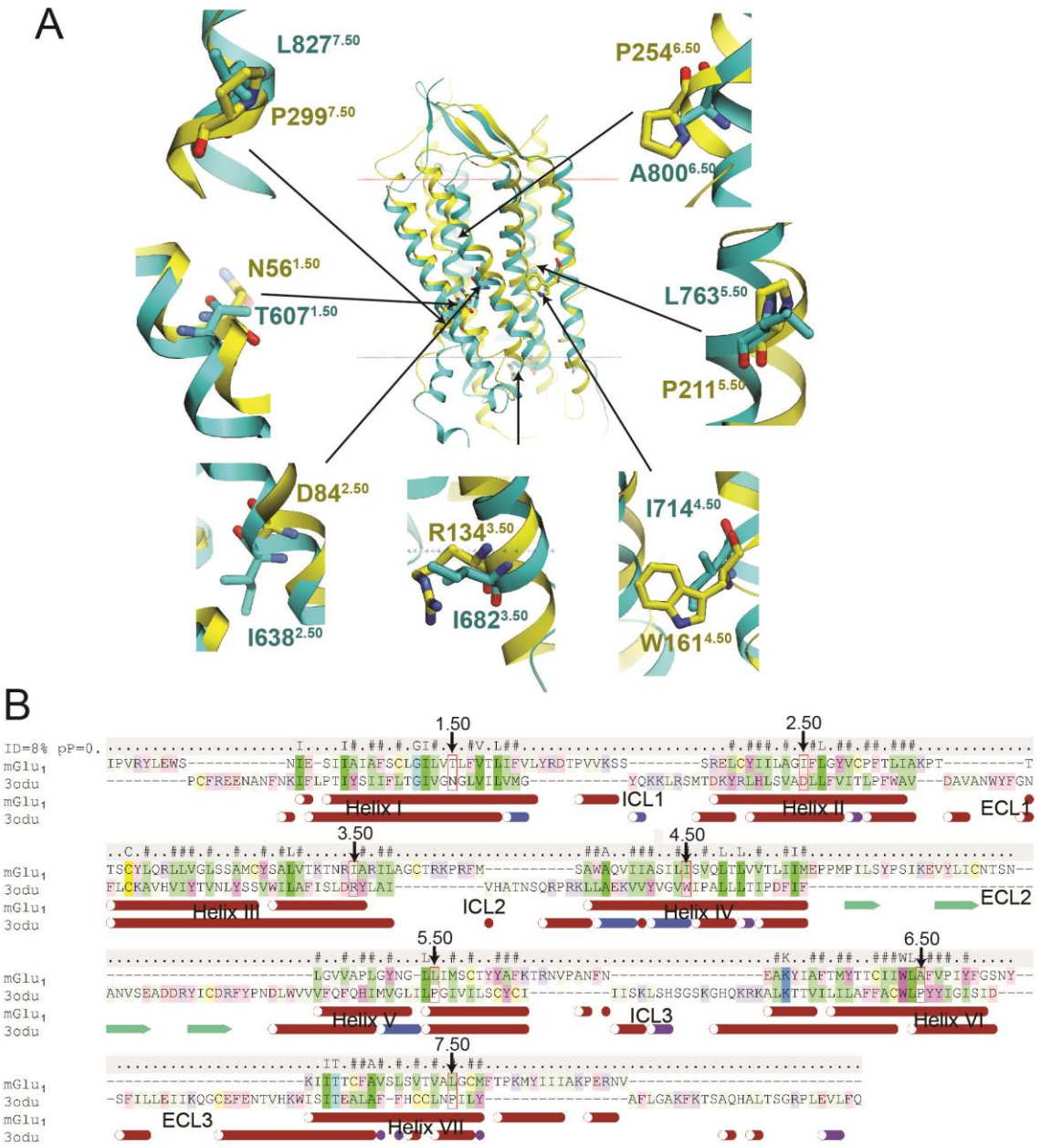

Fig. S8

Transplanting B&W numbering system to class C GPCRs. (A) Structural superposition of the human $mGlu_1$ (cyan) and human CXCR4 (PDB ID: 3ODU; yellow), obtained with the iterative structure alignment algorithm in ICM-Pro (Molsoft LLC). Inserts show details of superposition around the most conserved X.50 (B&W numbering) residues for each helix in class A GPCRs. (B) Sequence alignment based on the structural superposition of $mGlu_1$ and CXCR4. The structure of CXCR4 provided the best structural superposition with $mGlu_1$ among known GPCR structures (RMSD = 2.9 Å for the optimal superposition of $mGlu_1$ with 176 Cα atoms of CXCR4 transmembrane residues). Transmembrane helices in both structures are shown below the sequences as red (canonical α-helix) and blue (non-canonical helix) cylinders, while β-hairpins are

shown as green stripes. The X.50 residues are marked by red boxes and arrows with the corresponding B&W numbers.

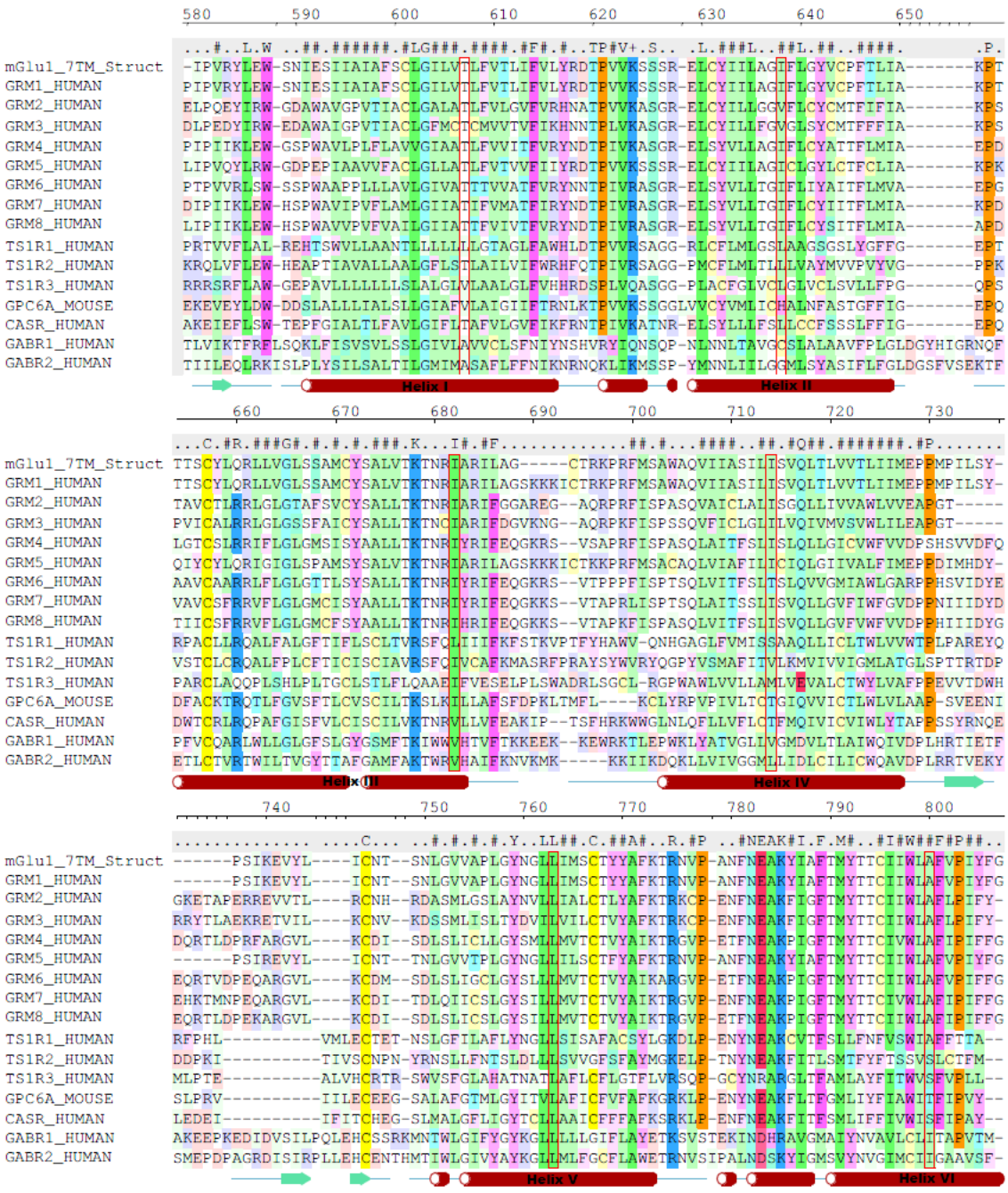
580
590
600
610
620
630
640
650
mGlu1_7TM_Struct
GRM1_HUMAN
GRM2_HUMAN
GRM3_HUMAN
GRM4_HUMAN
GRM5_HUMAN
GRM6_HUMAN
GRM7_HUMAN
GRM8_HUMAN
TS1R1_HUMAN
TS1R2_HUMAN
TS1R3_HUMAN
GPC6A_MOUSE
CASR_HUMAN
GABR1_HUMAN
GABR2_HUMAN
Helix I
Helix II
660
670
680
690
700
710
720
730
Helix III
Helix IV
740
750
760
770
780
790
800
Helix V
Helix VI

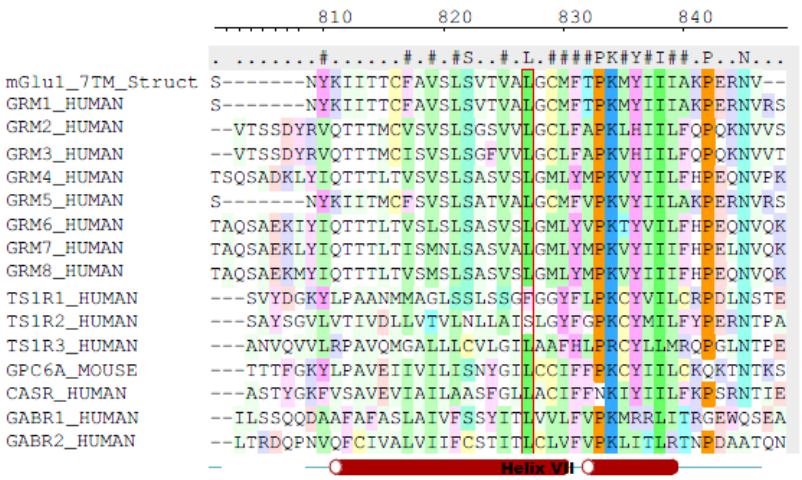

Fig. S9

Sequence alignment of human class C GPCR 7TM domains. Secondary structural elements in the human $mGlu_1$ 7TM structure are shown under the sequences. Residues at X.50 (B&W numbering) in class C GPCRs are shown in red boxes. Uncolored residues show lack of conservation, while coloring highlights conserved amino acids with specific functional properties (green: hydrophobic, blue: basic, red: acidic, magenta: aromatic, cyan: small polar, orange: proline, yellow: cysteine). The graphics were prepared using ICM molecular modeling package (Molsoft LLC).

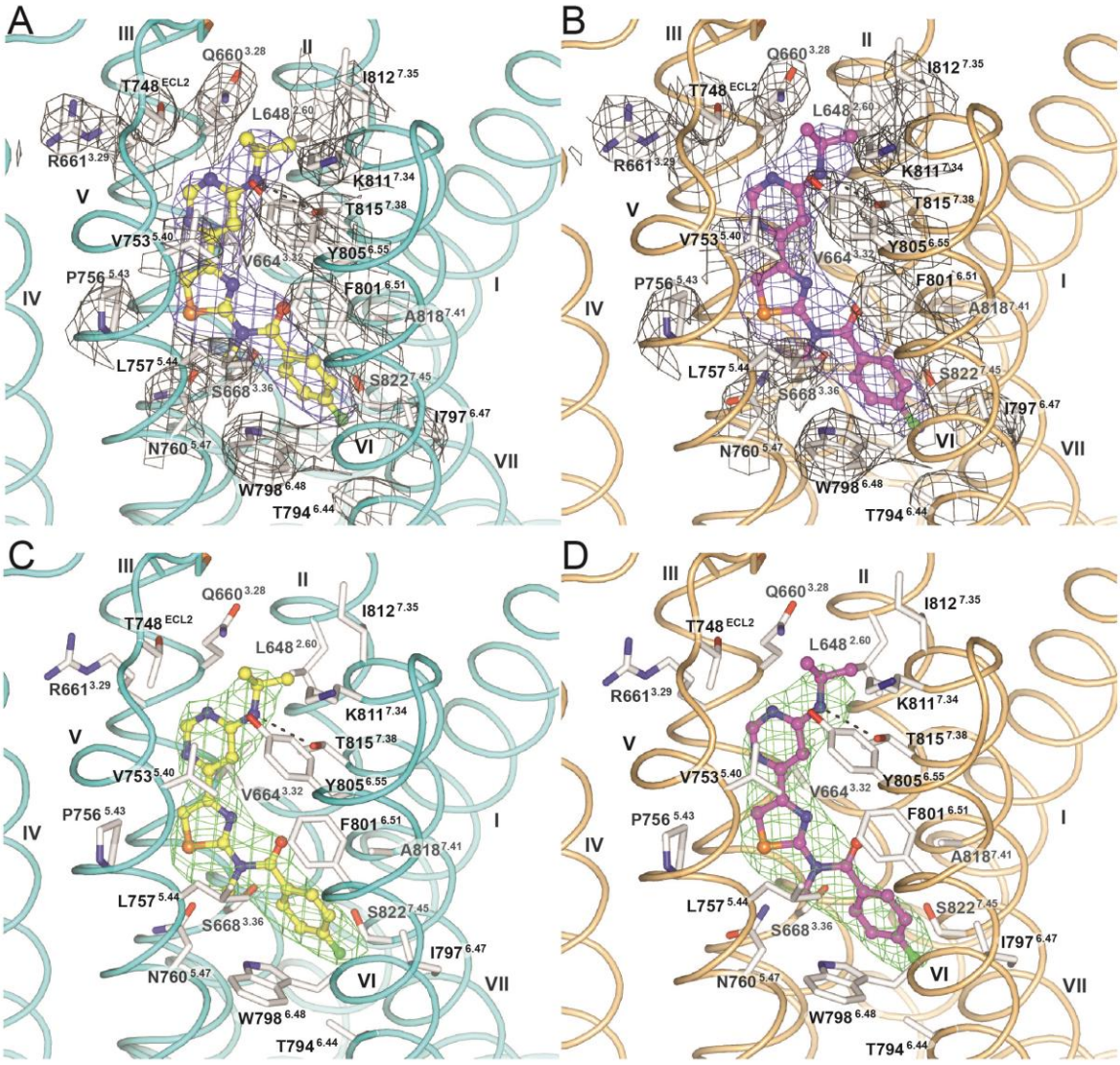

Fig. S10

Electron density maps of the ligand binding pocket. $|2F_O|-|F_C|$ maps (blue mesh for FITM and grey mesh for pocket residues) for the ligand binding pockets of molecule A (A) and molecule B (B) (contoured at 1.0σ, 0.10 e/ Å). $|F_O|-|F_C|$ omit maps (green mesh) of the ligand FITM in molecule A (C) and in molecule B (D) (contoured at 3.0σ, 0.15 e/Å). The backbone of molecule A is shown in cyan with ligand shown as yellow carbons. The backbone of molecule B is shown in light orange with ligand shown as magenta carbons. In both molecules, the side chains of ligand binding pocket residues are shown as white carbons. The images were created with PyMOL.

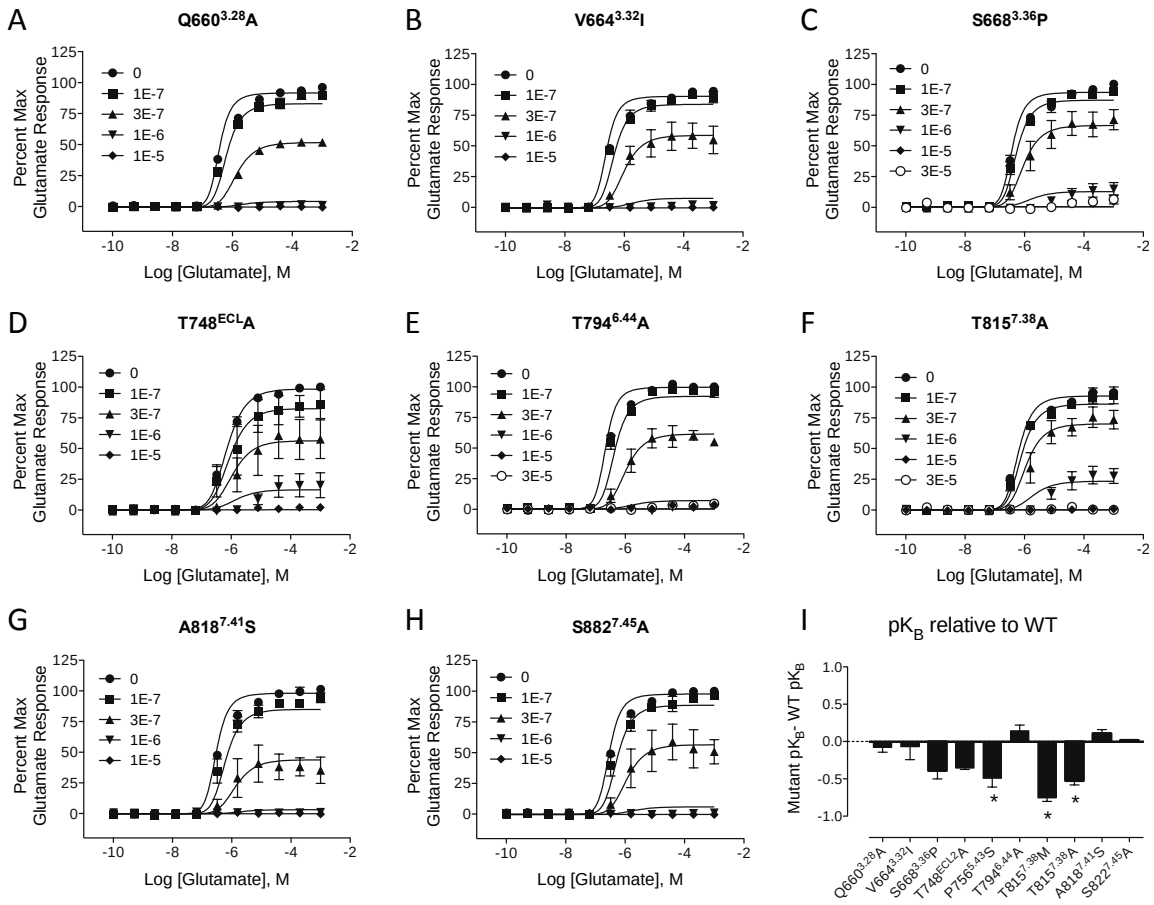

Fig. S11

Mutational analysis of FITM interactions with full-length human $mGlu_1$. Single point mutations in $mGlu_1$ were assessed for their effect on the affinity and cooperativity of FITM. Glutamate concentration response curves were performed in the absence and presence of the indicated concentrations of FITM at (A) $Q660^{3.28}A$, (B) $V664^{3.32}I$, (C) $S668^{3.36}P$, (D) $T748^{ECL2}A$, (E) $T794^{6.44}A$, (F) $T815^{7.38}A$, (G) $A818^{7.41}S$ and (H) $S822^{7.45}A$. The derived affinity and cooperativity estimates are summarized in Table S3. (I) The affinity (pK_B) of FITM was decreased ~3 fold at $P756^{5.43}S$ and $T815^{7.38}A$, and ~6 fold at $T815^{7.38}M$, compared to wild-type. * denotes $p < 0.05$ by one way ANOVA, Dunnett's post test. Data represent the mean ± S.E.M of three independent experiments performed in duplicate.

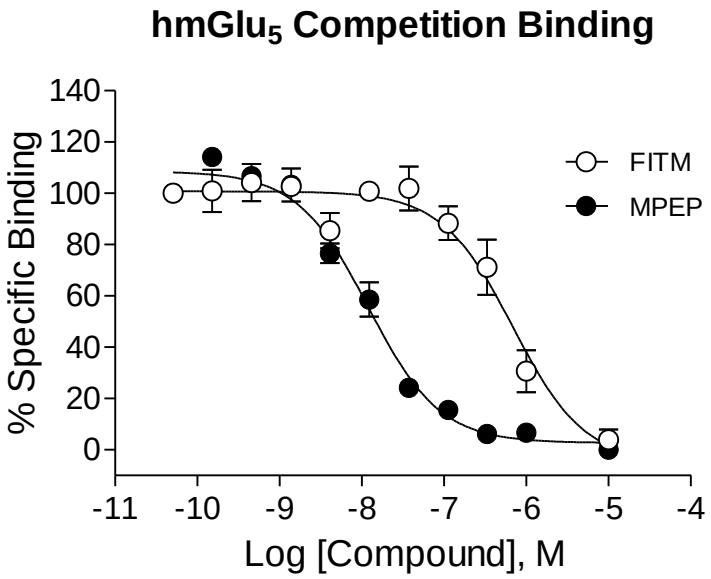

Fig. S12

FITM displaces an allosteric radioligand at human $mGlu_5$ with >100 fold lower affinity when compared to human $mGlu_1$. Competition binding was performed using HEK293A cell membranes stably expressing human $mGlu_5$. Increasing concentrations of FITM or MPEP (a reference $mGlu_5$ NAM) were incubated with 3 nM [^{3}H]-methoxyPEPy for 1 h at room temperature. FITM fully displaced [^{3}H]-methoxyPEPy with a K_i of 488 ± 107 nM and MPEP exhibited a K_i of 8.1 ± 1.5 nM. Data represent the mean ± SEM of three independent experiments performed in triplicate.

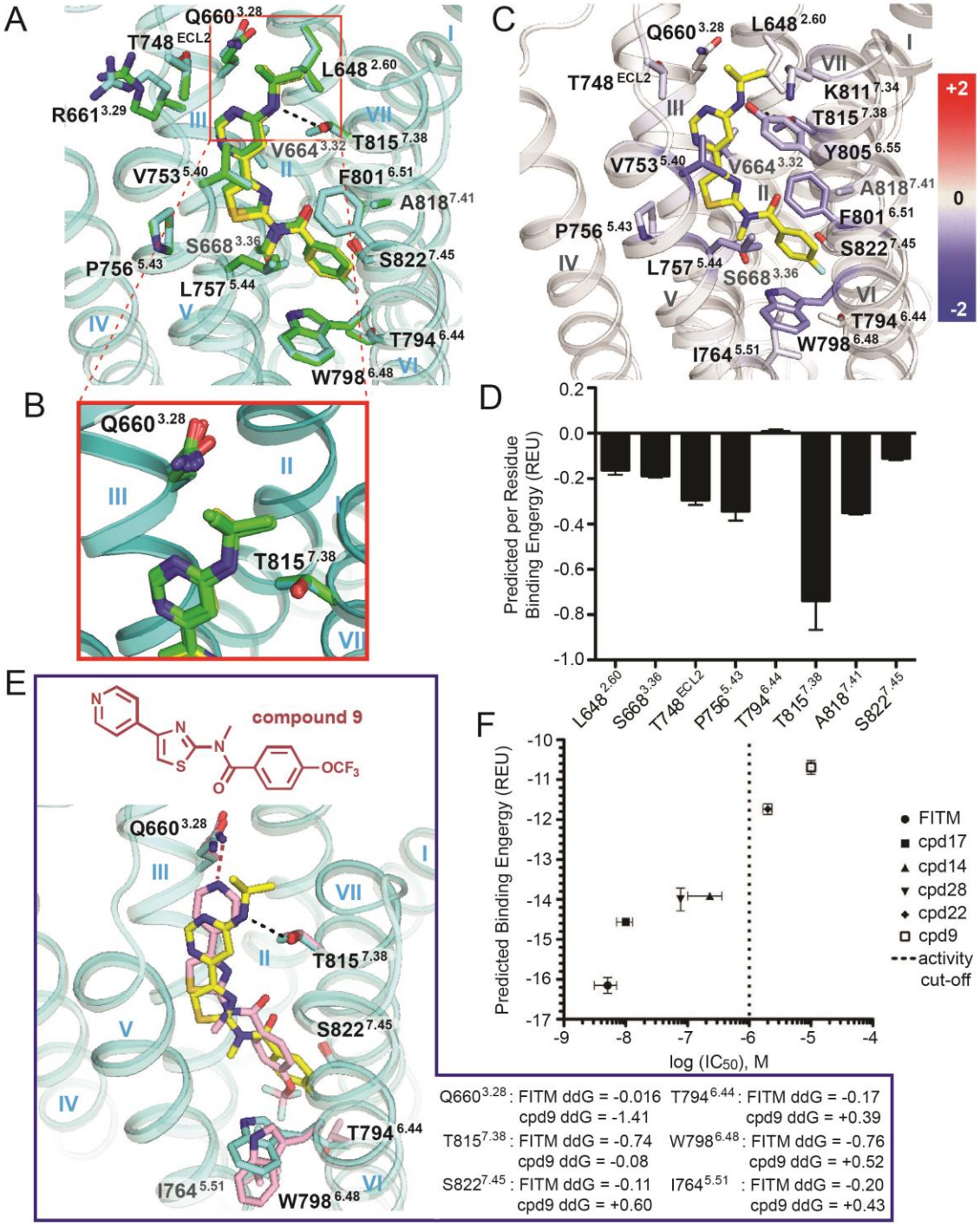

Fig. S13

Analysis of compound docking to human $mGlu_1$ 7TM crystal structure. (A) Re-docking FITM with RosettaLigand recapitulates the docking pose observed in the co-crystal structure with a RMSD of 0.3Å. (B) The $Q660^{3.28}$ side chain samples different rotamers. The $T815^{7.38}$ side chain conformation is strictly conserved, suggesting an essential role in interacting with ligand. (C) and (D) The important role of $T815^{7.38}$ in ligand binding is confirmed when comparing per-residue binding energies (ddG) as predicted by Rosetta in

Rosetta Energy Units (REU) which are represented as color scale in (C). (E) Compound 9 (salmon; IC_{50}: 10 μM) docked into the binding pocket lacks the capacity to interact with $T815^{7.38}$, and forms unfavorable interactions with $I764^{5.51}$, $T794^{6.44}$, $W798^{6.48}$ and $S822^{7.45}$ as indicated by ddG. Residues in the structure docked with compound 9 are shown in salmon. The crystal structure of $mGlu_1$ is shown in cyan, and the ligand FITM is shown in yellow. Hydrogen bonds between the receptor and the ligands are shown in dashed lines. (F) Correlation plot between log IC_{50} and Rosetta predicted binding energy for all the tested compounds and FITM. The Pearson correlation coefficient is 0.9704 (R square: 0.9418). The dashed line separates compounds considered active and inactive.

Table S1.

Data collection and refinement statistics. Highest resolution shell is shown in parentheses.

Structure	$mGlu_1$		
Data collection			
	Native	Ta_6Br_{12}	
Wavelength (Å)	1.0332	1.2548	1.0332
Space group	$P2_12_12_1$	$P2_12_12_1$	$P2_12_12_1$
Unit cell parameters a, b, c (Å)	67.36, 86.55, 168.28	67.24, 86.35, 169.65	67.44, 86.82, 168.69
Number of crystals	14	1	8
Number of reflections measured	149,517	46,976	43,735
Number of unique reflections	24,533	8,276	11,773
Resolution (Å)	50.0 – 2.8 (2.9-2.8)	50.0-4.0 (4.14-4.00)	50.0-3.5 (3.63-3.50)
R_{merge} (%)	13.2 (>100)	21.8 (>100)	12.9 (93.7)
Mean I/σ(I)	13.3 (1.3)	8.6 (1.5)	17.4 (2.0)
$CC_{1/2}$ [#]	0.973 (0.51)		
Completeness (%)	98.7 (96.1)	92.5 (83.0)	92.6 (95.0)
Redundancy	6.1 (5.8)	5.7 (4.2)	3.7 (3.8)
Phasing			
Figure-of-merit (FOM) after Density modification		0.66	
Refinement			
Resolution (Å) Number of reflections (test set)	50-2.80 24,480 (1,247)		
R_{work} / R_{free}	0.227 / 0.268		
Number of atoms Protein Ligand Lipids and other	A B 2,786 2,817 26 26 163 88		
Mean Overall B value (Å^2) $mGlu_1$ BRIL Ligand Lipids and other	A B 85.3 81.2 141.1 130.3 71.8 69.7 97.9 99.0		
R.m.s. deviations Bond lengths (Å) Bond angles (°)	 0.010 1.11		
Ramanchandran plot statistics (%)* Favored regions Allowed regions Disallowed regions	 97.5 2.5 0		

* As defined in MolProbity

Table S2.

Summary of operational model parameters for analysis of FITM allosteric interactions with glutamate at single point mutations of $mGlu_1$. Data are mean ± S.E.M from three independent experiments conducted with an N of 3-6 individual experiments.

construct	pK_B[a]	K_B (nM)	logβ[b]	logτ_A[c]
Wild-type	6.57 ± 0.04	266	-100	0.38 ± 0.02
$Q660^{3.28}A$	6.58 ± 0.01	265	-100	0.35 ± 0.01
$V664^{3.32}I$	6.58 ± 0.12	263	-100	0.45 ± 0.02
$S668^{3.36}P$	6.26 ± 0.16	548	-0.92[#]	0.25 ± 0.03*
$T748^{ECL2}A$	6.30 ± 0.05	505	-100	0.22 ± 0.07*
$P756^{5.43}S$	6.16 ± 0.17*	692	-0.60 ± 0.20	0.13 ± 0.00*
$T794^{6.44}A$	6.79 ± 0.02	162	-100	0.50 ± 0.04
$T815^{7.38}M$	5.82 ± 0.07*	1520	-0.24 ± 0.03	0.16 ± 0.04*
$T815^{7.38}A$	6.12 ± 0.07*	753	-100	0.23 ± 0.03*
$A818^{7.41}S$	6.76 ± 0.05	174	-100	0.41 ± 0.02
$S822^{7.45}A$	6.67 ± 0.07	214	-100	0.42 ± 0.03

a. Negative logarithm of the equilibrium dissociation constant (K_B) of FITM as derived using the operational model of allosterism.

b. The efficacy cooperativity parameter was constrained to -100 when complete blockade of glutamate was observed.

c. The transduction coefficient of glutamate, which is the ability of glutamate to activate the receptor.

*. Significantly different from wild-type value, $p<0.05$, one-way ANOVA, Dunnett's post-test.

#. In two of three experiments, incomplete blockade of the glutamate response was observed, the mean is reported.

Table S3.

The $mGlu_1$ binding pocket for FITM probably corresponds to the proposed common allosteric site for class C GPCRs. Summary of previous mutagenesis-based studies of class C GPCR allosteric sites shows that positions of the FITM binding pocket residues have also been implicated in binding of $mGlu_2$, $mGlu_5$, CaS and $GABA_B$ allosteric modulators. Although the $Y672^{3.40}$ side chain located at the bottom of the $mGlu_1$ allosteric pocket does not directly interact with FITM, mutation of this residue has been shown to impact binding of other $mGlu_1$ allosteric modulators, as well as binding of $mGlu_2$ and $mGlu_5$ allosteric modulators.

Parent	Mutant	B&W	Effect	Ref.
$mGlu_1$	*F599I [a] (r)[b]*	*1.42*	*Reduced potentiation by second site modulator: CPPHA, but not Ro 67-7476.*	*(28)*
	S668P (h)[c] *C671S (h)*	3.36 *3.39*	No gain of [^{3}H]MPEP binding (same as $mGlu_1$ wild-type); reduced potentiation by Ro 67-7476.	(*25*)
	S668P (h) *C671S (h)* *V823A (h)*	3.36 *3.39* *7.46*	Minimal amino acid $mGlu_{1\text{-}5}$ substitution to result in gain of [^{3}H]MPEP binding.	(*25*)
	Y672F (r)	*3.40*	*No effect on [^{3}H]EM-TBPC binding.*	*(23)*
	Y672V (r)	*3.40*	*Decreased [^{3}H]EM-TBPC affinity (>3 fold).*	*(23)*
	I725F (h)	*4.61*	*Decreased potency of CFMMC (~10 fold)*	*(22)*
	V757L (r)	5.44	Reduced potentiation by VU48 (PAM) and VU71 (PAM) and Ro 67-7476 (PAM); decreased [^{3}H]EM-TBPC affinity (10 fold) and potency.	(*23, 50, 60*)
	L757V (h)	5.44	Gain of potentiation by Ro 67-7476.	(*60*)
	V757A (r)	5.44	No effect on [^{3}H]EM-TBPC binding.	(*23*)
	N760A (h)	5.47	Decreased NAM potency of CFMMC (>30 fold), YM298198 and cpd1 (>3 fold); increased LY456066 NAM potency (>3 fold).	(*22*)
	W798A (h)	6.48	Increased CFMMC and LY456066 NAM potency; no effect on FTIDC NAM potency.	(*22, 61*)
	W798F (r)	6.48	Increased [^{3}H]EM-TBPC affinity (>3 fold) and potency.	(*23*)
	W798Y (r)	6.48	No effect on [^{3}H]EM-TBPC binding.	(*23*)
	F801A (h,r)	6.51	Loss of [^{3}H]EM-TBPC binding; decreased NAM potency of CFMMC, JNJ16259685 and cpd1 (>100 fold), FTIDC (>30 fold) and YM298198 switches to a PAM; decreased FTIDC potency (100 fold).	(*22, 23, 61*)
	Y805A (h,r)	6.55	Loss of [^{3}H]EM-TBPC binding and inhibition of glu function; decreased potency of CFMMC (>100 fold) and JNJ16259685, LY465066 and YM298198 (10 fold); no effect on FTIDC potency.	(*22, 23, 61*)
	T815M (h,r)	7.38	Decreased potency of CFMMC, JNJ16259685, LY465066 and YM298198 (>100 fold), FTIDC (>30 fold) and cpd1 (3 fold); loss of [^{3}H]EM-TBPC binding and no inhibition of glu function.	(*22, 23, 61*)
	T815M (h,r) A818S (h,r)	7.38 7.41	No effect on potentiation by VU48, VU71, Ro 67-7476; reduced inhibition by CPCCOEt, cyclothiazide and MPEP.	(*24, 26, 50*)

	A818S (r)	7.41	No effect on [^{3}H]EM-TBPC binding or NAM potency.	(*23*)
	A818I (r)	7.41	No effect on [^{3}H]EM-TBPC binding.	(*23*)
	V823A (h)	*7.46*	*No gain of [^{3}H]MPEP binding (same as wild-type mGlu$_1$).*	*(25)*
mGlu$_5$	*F585I (r)*	*1.42*	*Reduced potentiation by CPPHA (~3 fold reduction in CPPHA affinity), but not VU29; no effect on MPEP inhibition.*	*(28, 30, 31)*
	L634F (r)	2.60	No effect on second site modulator: CPPHA potentiation.	(*28*)
	R647A (r)	3.29	Decreased (>3 fold) [^{3}H]fenobam and [^{3}H]MPEP (<3 fold) affinity; no effect on MPEP or acetylene PAM affinity; no change in fenobam and MTEP NAM potency or inverse agonism of MPEP (PI); no effect on DFB potentiation.	(*23, 27, 31, 62*)
	R648E (h)	3.29	Decreased 2-BisPEB, 3-BisPEB and MPEP potency (3-10 fold); no effect on 4-BisPEB potency.	(*29*)
	I650A (r)	3.32	No effect on affinity of MPEP or acetylene PAMs.	(*31*)
	I651V (h)	3.32	No effect on [^{3}H]MPEP binding.	(*25*)
	I651F (h)	3.32	>30 fold decrease in 2-BisPEB, 3-BisPEB, 4-BisPEB and MPEP NAM potency.	(*29*)
	P654S (r)	3.36	Loss of [^{3}H]fenobam binding; decreased fenobam NAM potency (3-10 fold); >100 fold decreased MTEP potency; no effect on DFB potentiation of quisqualate; decreased VU0405398 affinity (>10 fold); >30 fold decreased [^{3}H]MPEP and VU0415051 affinity, decreased MPEP affinity (>10 fold) and NAM potency; loss of VU0360173 potentiation.	(*23, 27, 31, 62*)
	P655S (h)	3.36	Reduced [^{3}H]MPEP affinity and potency (3-10 fold); no effect on 2-BisPEB or 4-BisPEB potency; loss of 3-BisPEB inhibition.	(*25, 29*)
	P654F (r)	3.36	Decreased affinity of MPEP (>1000 fold), VU0415051, VU0403602, VU0405386 and VU0405398 (> 30 fold); loss of VU0360173 potentiation.	(*31*)
	P654S (r) *S657C (r)*	3.36 *3.39*	Decreased potentiation by DFB; loss of [^{3}H]fenobam binding; decrease potency of fenobam and MTEP (>100 fold); decreased [^{3}H]MPEP affinity (~10 fold).	(*23, 27, 62*)
	P654S (r) *S657C (r)* L743V (r)	3.36 *3.39* 5.44	Decreased DFB potentiation and gain of potentiation by mGlu$_1$ PAM: RO 67-7476.	(*60, 62*)
	P654S (r) L743V (r)	3.36 5.44	No effect on potentiation by DFB;	(*62*)
	S657C (r)	*3.39*	*No change in [^{3}H]MPEP affinity or MTEP potency; loss of [^{3}H]fenobam binding; >100 fold decrease in fenobam potency; loss of DFB potentiation; no effect on MPEP, VU0415051, VU0405398, VU0403602 and VU0405386 affinity.*	*(23, 27, 31, 62)*
	S658C (h)	*3.39*	*Reduced [^{3}H]MPEP affinity (3-10 fold).*	*(25)*
	Y658V (r)	*3.40*	*Loss of [^{3}H]fenobam and [^{3}H]MPEP binding; decreased MPEP potency and/or affinity (>30 fold), increased fenobam potency (>3 fold); no effect on DFB or VU0465731 potentiation; decreased affinity of VU0424465, VU0430644 and VU0405398 (>30 fold); loss of potentiation by VU0360172, VU0403602, VU0360173, VU0415051 and VU0405386; PAM to NAM switch for VU0405398 and VU0430644.*	*(23, 27, 30, 31, 62, 63)*
	Y658F (r)	*3.40*	*Decreased [^{3}H]fenobam affinity (3-10 fold) and potency (>10 fold); no effect on DFB potentiation or [^{3}H]MPEP affinity.*	*(23, 27, 62)*
	Y659F (h)	*3.40*	*Increased 4-BisPEB potency (~3 fold); no effect on 2-BisPEB, 3-BisPEB or MPEP potency.*	*(29)*
	Y659A (h)	*3.40*	*Decreased potency of 2-BisPEB (>10 fold) and MPEP (>100 fold); loss of inhibition by 3-BisPEB and 4-BisPEB.*	*(29)*
	V739M (r)	5.40	No effect on CPPHA potentiation or MPEP inhibition (at 10nM only).	(*28, 31*)

	P742S (r)	5.43	Decreased affinity of MPEP, VU360172 and VU0415051 (~3 fold), VU0403602 and VU0405386 (>10 fold); no effect on VU0360173 and VU0405398 affinity; increased cooperativity of acetylene PAMs.	(*31*)
	L743V (r)	5.44	Enhanced potentiation by DFB; no gain in potentiation by Ro 67-7476; increased positive cooperativity of VU29; no change in [^{3}H]fenobam affinity or potency of fenobam; ~3 fold decrease in [^{3}H]MPEP and MPEP affinity; no effect on acetylene PAM affinity.	(*30*, *31*, *62*)
	L743A (r)	5.44	No change in [^{3}H]fenobam affinity or potency; 3 fold decrease in [^{3}H]MPEP affinity and potency.	(*23*, *27*)
	N746A (r)	5.47	Decreased affinity of VU0403602 and VU0415051 (3-10 fold); no effect on MPEP, VU0360172, VU0360173, VU0405398 and VU0405386 affinity.	(*31*)
	N747A (h)	5.47	Decreased potency of MPEP and 2-BisPEB (>10 fold); loss of 3-BisPEB inhibition; no effect on 4-BisPEB.	(*29*)
	N747S (h)	5.47	Decreased potency of MPEP and 2-BisPEB (3-10 fold) and 3-BisPEB (>10 fold); no effect on 4-BisPEB.	(*29*)
	G747V (r)	*5.48*	*Decreased MPEP affinity (>3 fold), no effect on affinity of PAMs (VU0360172, VU0415051, VU0405386).*	(*31*)
	G748L (h)	*5.48*	*Reduced MPEP potency (>3 fold); no effect on 2-BisPEB, 3-BisPEB or 4-BisPEB.*	(*29*)
	T779A (r)	*6.43*	*Decreased MPEP affinity (~3 fold).*	*(31)*
	T780A (r)	6.44	Loss of [^{3}H]fenobam binding and DFB potentiation; decreased affinity of MPEP, VU0415051, VU0424465 and VU0405398 (>10 fold), VU0403602, VU0465731, VU0430644 (> 30 fold), VU0405386 (>100 fold); decreased fenobam potency (>30 fold); decreased [^{3}H]MPEP affinity (3 fold) and potency; loss of VU0360173 and VU0360172 potentiation; PAM to NAM switch for VU0415051.	(*23*, *27*, *31*, *62*, *63*)
	W784A (r)	6.48	Enhanced potentiation by DFB; loss of [^{3}H]fenobam binding; decreased fenobam potency (>100 fold); decreased MPEP affinity (>300 fold) and cooperativity; no effect on acetylene PAM affinity with the exception of VU0403602 (reduced ~10 fold); increased cooperativity of nicotinamide PAMs.	(*27*, *31*, *62*, *63*)
	W785A (h)	6.48	Decreased 4-BisPEB (~3 fold), 2-BisPEB (>10 fold) and MPEP (>100 fold) potency; 3-BisPEB potency unchanged.	(*29*)
	I783A (r)	6.47	No change in inhibition by MPEP (at 10nM only)	(*31*)
	W784F (r)	6.48	Enhanced potentiation by DFB; ~3 fold decrease in [^{3}H]MPEP and [^{3}H]fenobam affinity; fenobam potency decreased (<3 fold).	(*23*, *27*, *62*)
	F787A (r)	6.51	Loss of [^{3}H]fenobam and [^{3}H]MPEP binding; decreased MPEP (10 fold) and fenobam (>30 fold) potency; DFB switches to a NAM.	(*23*, *27*, *62*)
	F788A (h)	6.51	No effect on 2-BisPEB and 3-BisPEB potency; decreased MPEP potency (>10 fold); loss of 4-BisPEB inhibition.	(*29*)
	F788W (h)	6.51	Decreased potency of 2-BisPEB and MPEP (3-10 fold); loss of 3-BisPEB and 4-BisPEB inhibition.	(*29*)
	V788A (r)	*6.52*	*Decreased MPEP affinity (> 3 fold); increased affinity of PAMs: VU0360173 (>3 fold), VU0405398 (>30 fold), VU0415051 and VU0405386 (>10 fold).*	*(31)*
	Y791A (r)	6.55	Decreased DFB potentiation; decreased [^{3}H]fenobam and [^{3}H]MPEP affinity (>3 fold); decreased potency of fenobam (>30 fold) and MPEP (~10 fold).	(*23*, *27*, *62*)
	Y792A (h)	6.55	No effect on potency of 2-BisPEB; decreased MPEP and 4-BisPEB potency (3-10 fold); loss of 3-BisPEB inhibition.	(*29*)
	Y791F (r)	6.55	No effect on CPPHA potentiation or inhibition by MPEP (at 10nM only).	(*28*, *31*)
	Y792F (h)	6.55	No effect on potency of 2-BisPEB, 3-BisPEB, 4-BisPEB or MPEP.	(*29*)
	M801T (r)	7.38	No change in fenobam potency; loss of DFB potentiation.	(*27*, *62*)

	M802T (h)	7.38	No effect on [^{3}H]MPEP binding.	(*25*)
	M802T (h) S805A (h)	7.38 7.41	No effect on [^{3}H]MPEP binding; gain of inhibition by $mGlu_1$ NAM CPCCOEt.	(*24*)
	M802T (h) S805A (h) *A810V (h)*	7.38 7.41 *7.46*	Loss of [^{3}H]MPEP binding.	(*25*)
	S805A (h)	7.41	No effect on [^{3}H]MPEP binding.	(*25*)
	S808A (r)	7.45	Decreased affinity of VU0424465 (>10 fold), VU0465731, MPEP and VU0403602 (> 30 fold); no significant effect on affinity of VU0360172, VU0415051, VU0405398, VU0430644 or VU0405386; PAM to NAM switch for VU0405398 and VU0430644; PAM to neutral switch for VU0405386.	(*31*, *63*)
	S809A (h)	7.45	Decreased 2-BisPEB (>10 fold) and MPEP (> 30 fold) potency; no effect on 3-BisPEB or 4-BisPEB NAM potency.	(*29*)
	S808T (r)	7.45	Decreased affinity of MPEP (> 30 fold), VU0415051 and VU0403602 (~ 10 fold); no effect on VU0360172, VU0360173, VU0405398 and VU0405386 affinity.	(*31*)
	S809F (h)	7.45	Decrease in 2-BisPEB (>30 fold) and MPEP (> 300 fold) potency; no effect on 3-BisPEB or 4-BisPEB potency.	(*29*)
	A809V (r)	*7.46*	*Loss of [^{3}H]fenobam, [^{3}H]MPEP and [^{3}H]methoxyPEPy binding; decreased affinity of VU0360172 (>10 fold), MPEP (>100 fold), VU29, VU0403602, VU0405386 and VU0415051(>30 fold); decreased fenobam (>10 fold) and MPEP potency; decreased DFB potentiation, CPPHA not affected; loss of VU0360173 and VU0405398 potentiation.*	*(27, 28, 30, 31, 62)*
	A810V (h)	*7.46*	*Loss of [^{3}H]MPEP binding; decreased MPEP (>30 fold), 2-BisPEB (10 fold) and 4-BisPEB (>3 fold) potency; loss of 3-BisPEB inhibition.*	*(25, 29)*
	A809G (r)	*7.46*	*Decreased affinity of VU0415051, VU0405398 (> 10 fold), MPEP, VU0403602 and VU0405386 (> 30 fold).*	*(31)*
	A810G (h)	*7.46*	*Loss of [^{3}H]MPEP binding.*	*(25)*
	R635A (r)	3.28	Decreased RO4988546 (NAM) potency (>10 fold), no effect on RO5488608 (NAM); decreased inhibition of LY354740(orthosteric) binding by RO4988546 (>10 fold) and RO5488608 (>30 fold).	(*64*)
	R636A (r)	3.29	Decreased potency of RO5488608 (>100 fold) and RO4988546 (>3 fold); decreased inhibition of LY354740 binding by RO4988546 (>10 fold) and RO5488608 (>30 fold).	(*64*)
	L639A (r)	3.32	No effect on RO4988546 or RO5488508 NAM potency.	(*64*)
	F643A (r)	3.36	Decreased NAM potency of RO4988546 (>10 fold) but no effect on RO5488508; decreased inhibition of LY354740 binding by RO4988546 and RO5488608 (>3 fold).	(*64*)
$mGlu_2$	*Y647A (r)*	*3.40*	*No effect on RO4988546 or RO5488508 potency or inhibition of LY354740 binding.*	*(64)*
	S688L (h) *G689V (h)*	*4.51* *4.52*	*Reduced potentiation of glutamate by LY487379 and MRLSD-650.*	*(65, 66)*
	S688L (h) *G689V (h)* N735D (h)	*4.51* *4.52* 5.47	*Reduced potentiation of glutamate by LY487379 and MRLSD-650.*	*(65, 66)*
	G689V (h) N735D (h)	*4.52* 5.47	*Reduced potentiation of glutamate by LY487379 and MRLSD-650.*	*(65, 66)*

	H723V (h,r)	ECL2	No effect on potentiation by MRLSD-655 or LY487379; decreased potency of RO4988546 (>3 fold) and RO5488508 (>3 fold); reduced inhibition of LY354740 binding by RO4988546 (>3 fold), RO5488608 (>30 fold).	(*64-66*)
	H723F (r)	ECL2	Decreased potency of RO4988546 (~3 fold) and RO5488508 (>10 fold); reduced inhibition of LY354740 binding by RO4988546 (>3 fold) and RO5488608 (>30 fold).	(*64*)
	M728A (r)	5.40	No effect on RO4988546 or RO5488608 potency; no effect on inhibition of LY354740 binding by RO5488608; increased inhibition of LY343740 binding by Ro4988546.	(*64*)
	S731A (r)	5.43	No effect on NAM potency or inhibition of LY354740 binding by RO5488508; increased inhibition of LY343740 binding by RO4988546.	(*64*)
	L732A (r)	5.44	Decreased potency of RO4988546 (~10 fold) and RO5488508 (~30 fold); decreased inhibition of LY354740 binding by RO5488608 (>30 fold), but no effect on RO4988546.	(*64*)
	A733T (h) N735D (h)	*5.45* 5.47	Reduced potentiation of glutamate by LY487379 and MRLSD-650.	(*65, 66*)
	N735D (h,r)	5.47	Reduced potentiation by LY487379, BINA and MRLSD-650, but no effect on MNI compounds (NAMs); no effect on RO4988546 or RO5488508 potency; decreased inhibition of LY354740 binding (3-10 fold) for RO4988546 and RO5488608.	(*50, 64-66*)
	T769S (r)	6.44	No effect on RO4988546 or RO5488608 potency.	(*64*)
	T769V (r)	6.44	No effect on RO4988546 or RO5488608 potency.	(*64*)
	W773A (r)	6.48	Decreased RO4988546 potency (>100 fold), increased inhibition of LY354740 binding by RO4988546 (>3 fold) but no effect on RO5488608.	(*64*)
	W773F (r)	6.48	Decreased RO4988546 potency (~10 fold), no effect on RO5488508 potency; decreased inhibition of LY354740 binding by RO4988546 and RO5488608 (>3 fold).	(*64*)
	F780A (r)	6.55	Decreased RO4988546 potency (>3 fold), no effect on RO5488508 potency; decreased inhibition of LY354740 binding by RO4988546 and RO5488608 (>10 fold).	(*64*)
	M794A (r)	7.38	No effect on NAM potency or LY354740 binding by RO4988546 or RO5488608.	(*64*)
	V798A (r)	7.41	No effect on RO4988546 potency, decreased RO5488608 potency (>3 fold); decreased inhibition of LY354740 binding by RO4988546 and RO5488608 (>3 fold).	(*64*)
CaS	*S657Y (h)*	*2.49*	*Loss of expression mutant rescued by cinacalcet (PAM) and NPS-2143 (NAM); >3 fold decreased cinacalcet affinity.*	(*67*)
	F668A (h)	2.60	Reduced inhibition by NPS-2143 and potentiation by NPS R-568 (PAM).	(*68*)
	R680C (h)	3.28	Rescue of loss of expression mutant by cinacalcet and NPS-2143; no effect on cinacalcet affinity.	(*67*)
	R680H (h)	3.28	Rescue of loss of expression mutant by cinacalcet and NPS-2143; no effect on cinacalcet affinity.	(*67*)
	Q681H (h)	3.29	No effect on NPS-2143 affinity.	(*67*)
	F684A (h)	3.32	Reduced modulation by NPS-2143, NPS R-568 and calhex231; no effect on potentiation by calindol or NPS R-568.	(*68-70*)
	F684L (h)	3.32	Modest reduction in modulation by NPS R-568.	(*68*)
	F688A (h)	3.36	Reduced modulation by NPS-2143 and calhex231, no effect on PAM activity of calindol or NPS R-568.	(*69, 70*)
	L773R (h)	5.40	Reduced NPS-2143 affinity (~3 fold).	(*67*)
	L776A (h)	5.43	Increased potency of calhex231, no effect on NPS-2143, calindol or NPS R-568.	(*69, 70*)

	V817I (h)	6.47	No effect of cinacalcet or NPS-2143 on receptor expression.	(*67*)
	W818A (h)	6.48	Decreased potency of calhex231; no effect on modulation by calindol, NPS R-568 or NPS-2143.	(*69, 70*)
	F821A (h)	6.51	Increased potency of calhex231; no effect on NPS-2143; reduced PAM activity by calindol and NPS R-568.	(*69, 70*)
	F821L (h)	6.51	No effect of cinacalcet or NPS-2143 on expression of gain-of-function mutants.	(*67*)
	E837I (h)	7.38	Reduced modulation by NPS-2143 and NPS R-568.	(*68*)
	E837Q (h)	7.38	Reduced modulation by NPS R-568.	(*68*)
	E837A (h)	7.38	Reduced modulation by NPS-2143, calhex231, calindol and NPS R-568.	(*69, 70*)
	I841A (h)	*7.42*	*Reduced modulation by NPS-2143, calhex231, calindol and NPS R-568. potential mode switch to NAM for PAMs.*	*(69, 70)*
$GABA_{B2}$	A706T (r) *A708P (r)*	6.51 *6.53*	Gain of agonist activity of PAM: GS39783.	(*71*)
	A706T (r) *A708P (r)* S710T (r)	6.51 *6.53* 6.55	Gain of agonist activity of PAM: GS39783; can activate B2 subunit without co-expression of B1.	(*71*)

a. Italicized entries summarize the impact of mutations on residues not participating in the FITM binding pocket observed in the crystal structure of $mGlu_1$ 7TM domain.
b. (r) denotes rat parent construct;
c. (h) denotes human parent construct